Spectroscopic and Theoretical Study of $(CF_3SO_2)_2N^-$ ($TFSI^-$) and $(CF_3SO_2)_2NH$ (HTFSI)

I. Rey,[†] P. Johansson,[‡] J. Lindgren,[‡] J. C. Lassègues,*[,†] J. Grondin,[†] and L. Servant[†]

Laboratoire de Physico-Chimie Moléculaire (UMR 5803), Université Bordeaux I, 351 Cours de la Libération, 33405 Talence Cedex, France, and The Ångström Laboratory, Inorganic Chemistry, Box 538, Uppsala SE−75121, Sweden

Received: December 2, 1997; In Final Form: February 23, 1998

The vibrational properties of the $TFSI^-$ anion solvated in a polymer or in water have been studied by comparing its IR and Raman spectra with those of the HTFSI molecule. Ab initio self-consistent field Hartree−Fock calculations have also been performed on the free ion or molecule to investigate their Mulliken charges, equilibrium geometry, and internal force constants. Both experimental and theoretical approaches confirm a pronounced delocalization of the negative charge on the nitrogen and oxygen atoms and a marked double-bond character of the SNS moiety for the anion. This double-bond character is decreased for the HTFSI molecule, leading to rather distinct frequencies for some specific vibrations such as the stretching motions of the SO_2 and SNS groups. The agreement between experimental and calculated spectra is much better for HTFSI than for $TFSI^-$. Tentative explanations are proposed for this difference.

Introduction

Lithium bis(trifluoromethanesulfone)imide, $LiN(SO_2CF_3)_2$, abbreviated as LiTFSI, has received much attention in the field of polymer electrolytes.[1,2] Indeed, complexation of this salt with polyethers[3], polyimines,[4] or polyamides[5] gives on the average better conductivities than any other lithium salt. This is attributed to the low lattice energy of LiTFSI, the negative charge of the anion being delocalized on the nitrogen and four oxygens atoms. In addition, the shape and internal flexibility of this anion seem to induce a plasticizing effect and to reduce the crystallinity of linear polymers such as poly(ethylene oxide) (PEO).

After these first interesting observations, more detailed experimental and theoretical studies have appeared in the literature. The phase diagram of the PEO−LiTFSI system has been established;[6] structural information has been obtained on the pure salt[7] and on the $P(EO)_3$−LiTFSI complex;[8] infrared spectroscopy (IR) has been applied to $P(EO)_n$−$M(TFSI)_2$ (for M = Mg, Ca, Sr, Ba) complexes[9] and more recently to the $P(EO)_n$−LiTFSI system[10] and to a gel electrolyte−LiTFSI system.[11] A theoretical study of the $TFSI^-$ anion and of its ion pairing with Li^+ has also been published.[12]

The present authors have recently presented preliminary results obtained both from calculations of the potential energy surface and geometries of the free anion (two stable rotamers of C_1 and C_2 symmetry were obtained)[13] and from IR and Raman spectra of the $P(EO)_n$−LiTFSI complexes ($n \leq 6$).[14] However, discrepancies have appeared with some literature results. For example, values of 127° and 156° are calculated for the SNS angle of the free anion, respectively, by us[13] and by Arnaud et al.,[12] and our vibrational assignments in the region of the stretching modes of the SO_2 and CF_3 groups[14] differ from those of Wen et al.[10]

Therefore, we have tried in the present work to develop our previous investigations and to clarify the existing discrepancies. Calculations of Mulliken charges, geometries, and vibrational frequencies are presented for the free $TFSI^-$ anion and for the HTFSI molecule. IR and Raman spectra of $P(EO)_n$−LiTFSI complexes and of HTFSI are also reinvestigated and compared with the calculated spectra. We will explain below why we found it interesting to study the HTFSI molecule for comparison with its conjugate anion.

Experimental Section

IR and Raman Spectra. The $P(EO)_8$−LiTFSI complex is prepared by dissolving PEO (Aldrich MW 9×10^5) and adequate quantities of LiTFSI (Fluka) in dry acetonitrile. We have used for comparison another complexing polymer, Elvamide 8061 (Du Pont), which is a copolymer of nylon-6, nylon-6/6, and nylon-6/10. This amorphous copolymer, hereafter noted ELVA, is soluble in methanol. Elementary analysis has given the average formula $[CONH(CH_2)_{5.6}]_n$. The $(ELVA)_8$−LiTFSI complex has been prepared by dissolving the required quantities of salt and polymer in dry methanol.[5]

For the IR measurements, thin films of polymers and complexes are obtained by spreading a drop of solution on a silicon window. These films are heated and dried in situ in a vacuum chamber. The IR spectra are recorded as a function of the temperature with a Nicolet 740 spectrometer (4000−400 cm^{-1}) and with a Nicolet 20F (650−50 cm^{-1}) at a resolution of 4 cm^{-1}. Aqueous solutions of LiTFSI are studied in the mid-IR down to 750 cm^{-1} using the six reflections of a horizontal ATR device (SPECAC) equipped with a ZnSe crystal.

The IR spectrum of gaseous HTFSI has been recorded from the vapor pressure of the solid at room temperature, using a cylindrical glass cell of 17-cm path length equipped with KBr windows. HTFSI has been introduced in the cell under dry argon. We have recorded successive spectra as a function of time and observed that some absorption bands increase continuously to reach a maximum value after several hours. HTFSI has then been removed, and the cell was evacuated in order to record the spectrum of the windows alone. This spectrum is characteristic of the $TFSI^-$ anion, certainly associated with K^+

* To whom correspondence should be addressed
[†] Université Bordeaux I.
[‡] The Ångstrom Laboratory.

S1089-5639(98)00375-2 CCC: $15.00
Published on Web 04/15/1998

TABLE 1: Frequencies and Vibrational Assignment of $TFSI^-$ Solvated in Various Media[a]

	IR			Raman		
assignment	PEO	H_2O	ELVA	PEO	H_2O	ELVA
$\nu_a^{i.p.}\cdot SO_2$	1354 (76)	1354 (40)	1352 (66)	1349 (4)	1351 (2)	1353 (5)
$\nu_a^{o.p.}\cdot SO_2$	1334 (48)	1330 (27)	1330 (41)	1331 (5)	1330 (3)	1330 (4)
$\nu_s CF_3$	1240 (3)	1237 (2)	1242 (3)	1240 (42)	1239 (32)	1241 (33)
$\nu_a CF_3$	1227 (45)	1225 (32)	1226 (41)			
	1195 (100)	1198 (100)	1195 (100)	1192 (4)	1203 (2)	1194 (4)
$\nu_s^{o.p.}\cdot SO_2$	1136 (71)	1139 (49)	1137 (45)			
$\nu_s^{i.p.}\cdot SO_2$		1133 (51)		1137 (23)	1131 (23)	1132 (21)
$\nu_a SNS$	1060 (71)	1056 (65)	1059 (47)			
νCS	788 (11)	794 (7)	790 (9)			
$\nu_s SNS$[b]	761 (5)	766 (4)	763 (7)	762 (3)		
$\delta_s CF_3$[b]	739 (9)		741 (14)	740 (100)	744 (100)	742 (100)
δSNS	655 (11)		653 (15)	652 (2)		
$\delta_a^{o.p.}SO_2$	618 (43)		616 (31)			
$\delta_a^{i.p.}SO_2$	604 (26)		602 (21)	592 (5)	594 (5)	593 (5)
$\delta_a CF_3$	571 (27)		570 (22)	571 (8)	567 (6)	570 (6)
$\delta_s SO_2$				551 (8)	551 (9)	551 (7)
$\delta_a CF_3$	512 (23)		512 (18)			
ωSO_2	405 (8)			404 (11)	407 (13)	406 (11)
ωSO_2				398 (10)	401 (15)	401 (12)
τSO_2	359 (7)			352 (8)	351 (9)	340 (14)
				339 (17)	339 (16)	
ρSO_2	326 (7)			326 (28)	325 (20)	325 (21)
				312 (22)	312 (19)	312 (18)
ρCF_3	288 (7)			279 (42)	276 (45)	277 (35)
	224 (4)					
				170 (6)		
tCF_3				122 (10)		

[a] The numbers in parentheses indicate the relative height of each band. The symbols have their usual meaning: ν, stretching; δ, bending; ω, wagging; τ, twisting; ρ, rocking; t, torsion. [b] Assignments transposed in Table 6 (theoretical results). See also discussion in the comparison section.

and resulting from a reaction of HTFSI with the KBr windows. It can be used as a background for the previous gas-phase spectra with an appropriate subtraction factor. A unique spectrum of gaseous HTFSI is then obtained. The observed frequencies are practically the same as those reported by Foropoulos et al.[15] using a 10-cm gas cell with AgCl or KCl windows.

For the Raman study of the $P(EO)_8$−LiTFSI and $(ELVA)_8$−LiTFSI complexes, films are obtained by casting the solution on a flat poly(tetrafluoroethene) surface. Most of the solvent is evaporated under ambient air until a self-supported membrane can be removed. Then, the membranes are treated for 24 h under vacuum at 60 °C to remove the last traces of solvent and stored in a drybox under argon atmosphere. The Raman spectra of these films are recorded as a function of the temperature using a heating Linkam THMSG600 stage flushed with argon and a LabRam-Dilor spectrometer (He/Ne 632.8-nm exciting line, CCD detector, holographic notch filter, Olympus BH2 microscope, 50× objective, spectral resolution 4 cm^{-1}). The Raman spectrum of solid HTFSI were also recorded for comparison.

All the IR and Raman spectra of polymer−salt complexes have been brought to a similar intensity scale by setting the integrated intensity of the δ CH_2 band between 1415 and 1510 cm^{-1} to a constant value.

Computational Methods. In an earlier paper two stable structures of the TFSI anion were found from quantum mechanical calculations.[13] The C_2 geometry of the TFSI anion from that paper has been optimized by ab initio Hartree−Fock (HF) self-consistent field (SCF) molecular orbital calculations with the 6-31G* basis set using the GAUSSIAN94 program.[16] For the geometry optimization of the HTFSI molecule, the 6-31G** basis set is used, giving p polarization functions on hydrogen apart from the d functions on the heavy atoms. The vibrational frequencies, IR intensities, and Raman activities are calculated for the structures obtained. The potential energy distribution (PED) matrix and the internal force constants are calculated with the GAMESS program.[17] The geometry used in GAMESS for the HTFSI acid differs slightly from the one obtained by GAUSSIAN94 owing to a different choice of p polarization functions. The Spartan program[18] is used to visualize the modes. The assignments in the tables are, however, based on the PED, since many modes are too complex to unambiguously be described in terms of group vibrations, as could be detected by viewing the modes.

Spectroscopic Results and Discussion

Assignments and measured wavenumbers for the systems containing the TFSI anion are given in Table 1 and those for HTFSI in Table 2. The assignments are based on comparison with similar systems. A more detailed assignment in terms of internal coordinates is presented below in the Theoretical Results and Discussion section.

IR and Raman Spectra of the Solvated $TFSI^-$ Anion. The dielectric constant of the complexing polymers PEO ($\epsilon \sim 5$) and ELVA ($\epsilon \sim 3$) at room temperature is much lower than that one of water ($\epsilon \sim 80$). As a result, it is well-known that ionic associations are favored in polymer electrolytes.[19−21] With increasing salt concentration, ion pairs (Li^+X^-), triplets (LiX_2^- or Li_2X^+), quadruplets (Li_2X_2), and even higher aggregates can appear. The magnitude of these effects depends also strongly on the basicity of the anion. Thus, several IR and Raman studies have shown that ion-pairing effects appear quickly in $P(EO)_n$−$LiSO_3CF_3$[19,20] and even for dilutions as high as $n = 4820$ in poly(propylene glycol)$_n$−$LiSO_3CF_3$[22] but here OH end groups may influence the results. On the other hand, this phenomenon seems to be much less pronounced in $P(EO)_n$−LiTFSI complexes. We have previously found that their vibrational spectra do not exhibit any indication of ion−ion interactions for $n = 8$.[14] IR studies of $P(EO)_n$−$M(TFSI)_2$ complexes (with M =

TABLE 2: Frequencies and Vibrational Assignment of HTFSI

HTFSI gas IR		HTFSI solid Raman		
Foropoulos et al.[15]	this work	Foropoulos et al.[15] −180 °C	this work 25 °C	assignment
3395 (m)	3394 (15)	3205 (w)	3197 (13)	
3320 (br)				νNH
		1464 (vw)	1456 (1)	
1463 (m)	1463 (78)	1458 (w)	1443 (4)	
1440 (m)	1442 (6)	1450 (w)	1436 (5)	$\nu_a SO_2$
			1427 (2)	
	1326 (2)	1343 (w)	1332 (3)	δNH
1300 (w)	1301 (21)	1263 (s)	1250 (73)	$\nu_s CF_3$
1240 (s)	1241 (100)			
1224 (s)	1225 (66)		1220 (3)	$\nu_a CF_3$
	1200 (10)		1208 (3)	
1138 (s)	1140 (70)	1142 (m)	1134 (26)	$\nu_s SO_2$
860 (m)	859 (80)	839 (w)	830 (8)	ν_aSNS
	768 (0.5)	778 (s)	765 (100)	$\delta_s CF_3$
643 (vw)	647 (0.5)	646 (w)	634 (5)	δSNS
614 (m)	615 (55)	591 (w)	583 (10)	$\delta_a SO_2$
570 (vw)	570 (5)	566 (w)	570 (7)	$\delta_a CF_3$
505 (w)	503 (14)		555 (8)	
	460 (3)	537 (w)	526 (3)	γNH
		510 (w)	495 (3)	
		392 (m)	380 (18)	
		386 (m)		
		346 (s)	335 (28)	
		311 (s)	299 (29)	
		276 (s)	264 (45)	
		212 (w)	210 (2)	
		195 (w)	202 (3)	
		128 (m)	185 (5)	

[a] The relative intensities are indicated in parentheses.

Mg, Ca, Sr, and Ba) show that contact ion pairs are formed for only $n = 7$.[9] A recent study of gel electrolytes containing LiTFSI[11] indicates that no contact ion pairs are formed for 0.5 and 1 M solutions whereas an increase to 5 M results in substantial ionic association. The ion pairing could in this case be monitored by IR spectroscopy from TFSI band shifts of three bands in the 730−800 cm^{-1} region.

Such a peculiar behavior for LiTFSI can be associated with the extensive charge delocalization and weak coordinating power of TFSI$^-$ compared to that of $CF_3SO_3^-$, but it can also be argued that the relatively low symmetry of TFSI$^-$ makes the spectroscopic analysis less sensitive than that for $CF_3SO_3^-$. Actually, an indirect confirmation of negligible ion−ion interactions in P(EO)$_n$−LiTFSI for $n > 8$ has been provided by in situ Raman measurements on a symmetric lithium cell using this electrolyte at 80 °C:[23−25] when a constant current is passed through the cell, linear salt concentration profiles have been observed between the two electrodes at the steady state, in agreement with the hypothesis of a fully dissociated salt.

As we want to correlate experimental observations and theoretical calculations on a "free" TFSI$^-$ anion, we will consider only polymer−LiTFSI complexes with $n = 8$ and diluted aqueous solutions. More complete data as a function of salt concentration and temperature can be found in the preceding paper.[14] The IR and Raman spectra of the polymer complexes, pure polymers, and aqueous solution are compared in Figures 1 and 2 between 1500 and 1000 cm^{-1}, i.e., in the spectral range where the stretching vibrations of the SO_2 and CF_3 groups occur. All these spectra are obtained at 25 °C except those of PEO and of P(EO)$_8$−LiTFSI, which are run at 80 °C in order to melt these compounds and to avoid any problem of crystalline-phase separation.[6] After subtraction of the solvent contribution, the difference spectra of Figure 3 are obtained.

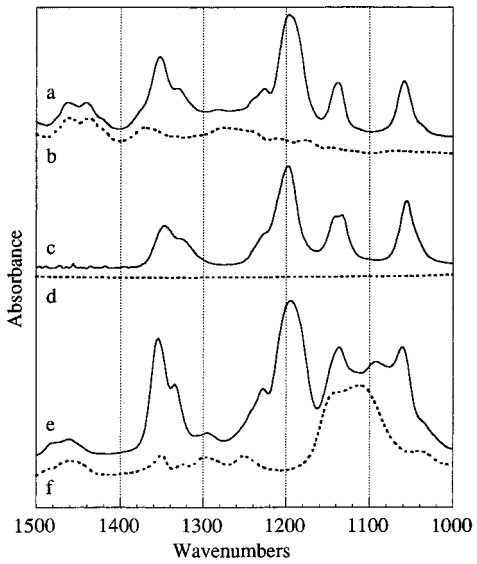

Figure 1. Infrared spectra of (ELVA)$_8$−LiTFSI (a), ELVA (b), (H$_2$O)$_{266}$−LiTFSI (c), H$_2$O (d), P(EO)$_8$−LiTFSI at 80 °C (e), and PEO at 80 °C (f).

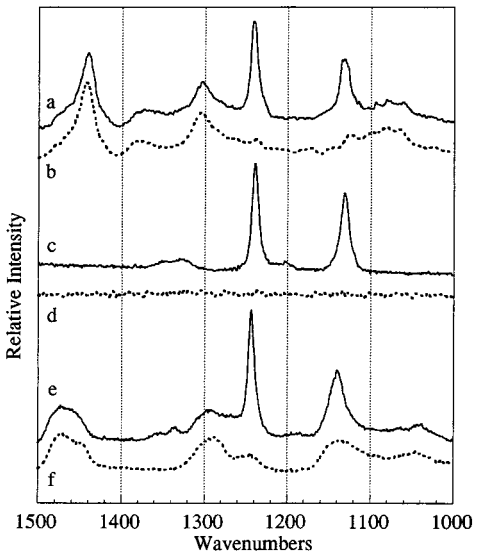

Figure 2. Raman spectra of (ELVA)$_8$−LiTFSI (a), ELVA (b), (H$_2$O)$_{266}$−LiTFSI (c), H$_2$O (d), P(EO)$_8$−LiTFSI at 80 °C (e), and PEO at 80 °C (f).

All fundamental vibrations of the TFSI$^-$ anion are situated below 1400 cm^{-1}. If the anion adopts a C_2 symmetry, its 39 internal vibrations can be classified into 20 A and 19 B modes, the former being polarized in Raman. According to literature data on similar systems,[26−30] the antisymmetric stretching mode of the SO_2 groups, $\nu_a SO_2$, is expected between 1300 and 1350 cm^{-1} and the symmetric one, $\nu_s SO_2$, between 1120 and 1160 cm^{-1}. In addition, for C_2 symmetry, each of these modes would be split into in-phase (A) and out-of-phase (B) components because of coupling between the two SO_2 groups. In the IR spectra, we observe effectively a broad and structured envelope with at least two components at about 1330 and 1350 cm^{-1}, whereas two weak signals appear at the same frequencies in Raman but with a reverse relative intensity (Figure 3). In aqueous solution, the high-frequency component is found to be polarized and therefore it is assigned to the $\nu_a^{i.p.} SO_2$ component of A symmetry (i.p. = in-phase). Thus, the low-frequency component corresponds to $\nu_a^{o.p.} SO_2$ of B symmetry (o.p. = out-of-phase). As seen in Figure 3 and Table 1, the frequencies of these modes vary by only a few cm^{-1} in the different solvents.

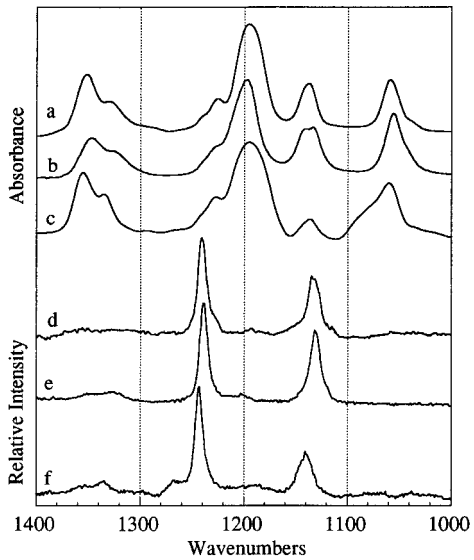

Figure 3. Infrared spectra (a, b, c) and Raman spectra (d, e, f) of $(ELVA)_8$−LiTFSI (a and d), $(H_2O)_{266}$−LiTFSI (b and e), and $P(EO)_8$−LiTFSI at 80 °C (c and f) after subtraction of the solvent.

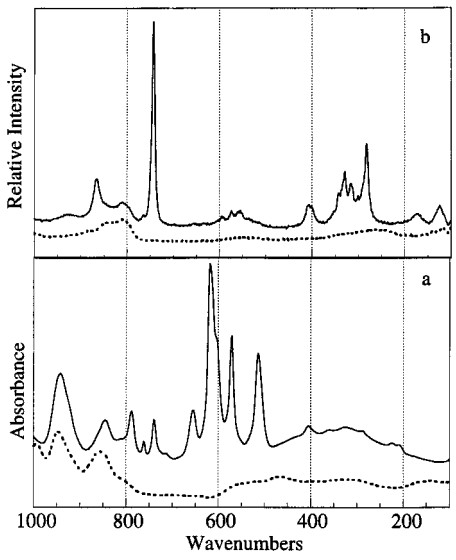

Figure 4. Low-frequency infrared and Raman spectra of PEO (dotted line) and of $P(EO)_8$−LiTFSI (solid line) at 80 °C.

Similarly, the IR band at 1130−1140 cm^{-1} due to νsSO_2 is weakly solvent-dependent. Two components can still be distinguished in aqueous solution at 1139 and 1131 cm^{-1}. The Raman spectra exhibit only a single intense and polarized line at 1131 cm^{-1}. Therefore, this low-frequency component is assigned to $\nu_s^{i.p.}SO_2$ (A) and the high-frequency one to $\nu_s^{o.p.}SO_2$ (B).

Between 1160 and 1270 cm^{-1}, the IR spectra exhibit a very intense absorption with a main maximum at 1195 cm^{-1} and a shoulder at 1225 cm^{-1}, assigned to ν_aCF_3. The Raman spectra present a strong polarized line at 1240 cm^{-1}, which is assigned to ν_sCF_3 (Table 1).

Finally, in the frequency range of Figure 3, one is left with an intense IR absorption at 1060 cm^{-1} having no Raman counterpart. A similar IR band has systematically been observed with other salts of $TFSI^-$ (Mg, Ca, Sr, Ba) complexed with PEO, but its origin has not been clarified.[9] We have proposed to assign it to the antisymmetric stretching mode of the SNS group, ν_aSNS, the high-frequency value of this mode being justified by the partial double-bond character of the SNS group in the anion.[14]

One of the main reasons why we have used ELVA in addition to PEO can be seen in Figure 1: in the 1000−1200 cm^{-1} region, PEO exhibits rather strong IR absorptions (νCOC vibrations) whereas ELVA does not. The accuracy of the subtraction is thus much better with the latter polymer, and Figure 3 shows that the ν_sSO_2 and ν_aSNS profiles are very similar in ELVA and in water. The shoulder that appears at about 1080 cm^{-1} in PEO (Figure 3c) is likely to come from a νCOC mode of the complexed polymer.

For the IR and Raman spectra between 1000 and 50 cm^{-1} (Figure 4), vibrational assignments become more difficult because the concept of group frequency is even less satisfying than above. Some propositions, based on literature data on similar systems, are however given in Table 1. In particular, the more intense Raman line at 740 cm^{-1} is assigned to δ_sCF_3 and the more intense IR one at 618 cm^{-1} to δ_aSO_2. Actually, the latter presents a shoulder at 604 cm^{-1}, which corresponds to a weak Raman line at about the same frequency. We are tempted to assign this shoulder to $\delta_a^{i.p.}SO_2$ and the main band at 618 cm^{-1} to $\delta_a^{o.p.}SO_2$. In this wavenumber region the two calculated rotamers differ in their vibrational pattern, and one of the observed bands at 618 and 604 cm^{-1} might originate from the C_1 rotamer. The nature of these vibrations will be more precisely discussed by comparison with the theoretical calculations. Let us simply point out two interesting features of the $P(EO)_8$, LiTFSI complex not included in the calculations:

A broad IR absorption centered at about 300−350 cm^{-1} is observed in the complex (Figure 4a). It reflects the vibrations of the cation in its solvating cage ("rattling" motion). It has already been observed at about the same frequency in other PEO/Li^+ complexes and substitution of Li^+ by Na^+ or K^+ has been shown to shift this absorption to about 180 and 150 cm^{-1}, respectively.[31,32] Similar features have also been reported for complexes of branched poly(ethylene imine) with lithium or sodium salts.[5]

A Raman line, not present in pure PEO, appears in the complex at 862 cm^{-1} (Figure 4b). This line corresponds to the so-called "breathing mode" of a PEO segment solvating Li^+ and adopting a kind of crown-ether-like conformation.[31,32] We have found that the integrated intensity of this line, normalized by the integrated intensity of the δCH_2 band of PEO, increases linearly with $1/n = [Li]/[EO]$ for $n > 8$.[23−25] One can infer that in this concentration range the lithium has a constant number of solvating ether oxygens.

IR and Raman Spectra of the HTFSI Molecule. To confirm some of the assignments proposed for the $TFSI^-$ anion, in particular concerning the very important SNS and SO_2 vibrations, we have studied the HTFSI molecule. Indeed, strong but variable electronic delocalization is known to occur within the approximately tetrahedral NSO_2R groups of $(RSO_2)_2NX$ systems, depending on the nature of R = F, CH_3, C_2H_5, CF_3, C_6H_5, ... and of X = H or a monovalent cation. It has been shown in particular that the molecules with R = F or CF_3 and X = H rank among the strongest neutral Brønsted acids.[15,33,34] When they are deprotonated, i.e., when H is replaced by a monovalent cation such as Li^+, electron delocalization from planar, sp^2-hybridized nitrogen into 3d sulfur orbitals is still increased, resulting in even shorter SN bonds and in a slight lengthening of the SO bonds. The values reported in Table 3 for some characteristic bond angles and lengths illustrate these effects.[7,12,33−41] The double-bond character of the SNS moiety can be evaluated by comparing the S−N distances of 1.58 ± 0.02 and 1.64 ± 0.02 Å found for the anions and acids,

TABLE 3: Selected Bond Lengths and Angles for Various $(RSO_2)_2NX$ Compounds

ion or molecule	d(S−N) (Å)	d(S═O) (Å)	a(SNS) (deg)	a(OSO) (deg)	ref
$(CF_3SO_2)_2N^-Li^+$	1.557	1.451, 1.429	129	118	7
$(CF_3SO_2)_2N^-$ [b]	1.520	1.439, 1.441	156.2	118.1	12
$(CH_3SO_2)_2N^-$	1.59		122		35
$(CF_3SO_2)_2N^-[Mg(H_2O)_6^+]\cdot 2H_2O$	1.577[a]	1.412[a]	125	117.7, 121.0	33
$(CF_3SO_2)_2NH$	1.644	1.401, 1.417	128.4	123.9	33
$(CH_3SO_2)_2NH\cdot H_2O$	1.645	1.428	125		36
$(C_2H_5SO_2)_2NH$	1.645	1.422	125.3		37, 38
$(C_6H_5SO_2)_2NH$	1.643, 1.647	1.415	127.7		39
$(FSO_2)_2NXeF$	1.623, 1.628	1.405	120.5		40
$(FSO_2)_2N^-(C_6H_5)_4As^+$	1.567	1.415	121.4		41
$(C_6H_5SO_2)_2N^-Na^+$	1.598, 1.571	1.446	127.5		39

[a] Average value. [b] Calculated value.

respectively, with the limiting value of 1.77 Å calculated from the covalent radii of the N and S atoms. It is remarkable that the SNS angle remains between 120 and 130° in the whole series of compounds.

It must be pointed out that the data of Table 3 concern solid compounds and some structural variations will occur for the free or solvated species when intermolecular forces are suppressed or decreased. Thus the HTFSI molecule in the gas phase at low pressures is not hydrogen-bonded, whereas the NH group in solid HTFSI is involved in a bifurcated hydrogen bond with two oxygens of a neighboring molecule.[33] This hydrogen bond is not very strong since $d(H\cdot\cdot O) = 2.26$ Å, but significant frequency shifts can be expected for the NH vibrations between the gas and solid states, even for small-bond length variations. Similarly, the cation in solid LiTFSI is coordinated in a tetrahedral manner by four oxygens from four different anions,[7] whereas one can infer that for $n = 8$, a concentration range where we have previously found ion-pairing effects to be negligible, Li^+ ions are mainly coordinated by ether oxygens and the $TFSI^-$ anion interacts very weakly with the polymer and cation. An indirect proof of this situation is provided by a transport number as high as 0.71 for the anion.[23−25] The average number of ether oxygens involved in the Li^+ complexation remains difficult to determine. Molecular dynamics simulations indicate a preference for the lithium to be coordinated by five oxygens of a single polymer strand forced into a crown-ether-like conformation.[42]

Returning to the spectroscopic comparison between $TFSI^-$ and HTFSI, since the double-bond character of the SNS bond is weaker in the latter, the ν_aSNS mode should occur at a lower frequency. It was situated at 875 cm^{-1} for $(CH_3SO_2)_2NH$.[27] Effectively, the IR spectrum of gaseous HTFSI reported in Figure 5a is quite different from those of the $TFSI^-$ anion (Figures 1−4). The band at 1060 cm^{-1} has disappeared, and a strong absorption is now present at 859 cm^{-1}. This new band is assigned to ν_aSNS in HTFSI. So, a lengthening of the S−N bond by about 0.09 Å between $TFSI^-$ and HTFSI has lowered ν_aSNS by 200 cm^{-1}. One can also notice that the νsSO_2 mode occurs at about the same frequency as in $TFSI^-$ but the νaSO_2 mode is shifted by more than 120 cm^{-1} to higher frequencies. Although frequency shifts are expected from the shortening of the S═O bonds from $TFSI^-$ to HTFSI (Table 3), the observed changes cannot be simply rationalized without considering coupling effects with other vibrational modes. These coupling effects will be directly taken into account in the theoretical approach. It is noteworthy that the νaSO_2 and νsSO_2 IR bands in gaseous HTFSI are relatively narrow and symmetric; they do not exhibit the splitting previously discussed for $TFSI^-$.

We could not obtain the Raman spectrum of gaseous HTFSI, but the Raman spectrum of the solid can usefully be compared to the IR one (Figure 5 and Table 2). In particular, a well-

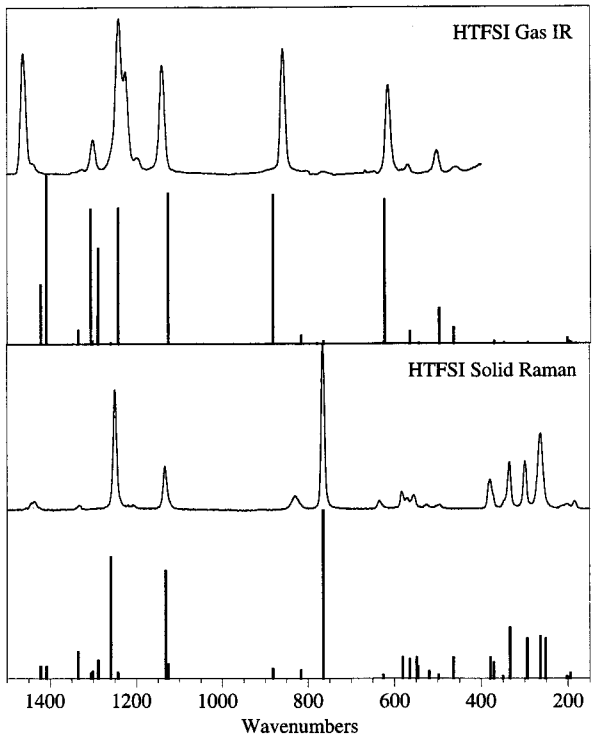

Figure 5. Vibrational spectra of HTFSI, (a) gas phase in infrared; (b) solid phase in Raman and comparison with the calculated IR and Raman spectra of the isolated HTFSI molecule.

isolated νNH vibration, not represented in Figure 5 for simplicity, is observed at 3394 cm^{-1} in the gas state; it is shifted to 3197 cm^{-1} in the solid as a result of the formation of N−H···O hydrogen bonds.[33] The in-plane deformation mode, δNH, is assigned to the 1326 cm^{-1} weak IR absorption and to the 1332 cm^{-1} Raman line. The out-of-plane deformation mode, γNH, is situated at 460 cm^{-1} in the gas state, and we expect a frequency increase in the solid state; there are two possible candidates at 495 and 526 cm^{-1} (Figure 5b, Table 2).

In the Raman spectrum of the solid, the strong lines at 1134 and 1250 cm^{-1} are easily assigned to the νsSO_2 and νsCF_3 vibrations, respectively. The νaSO_2 mode gives a weak doublet at 1436 and 1443 cm^{-1}. We assign the more intense Raman line at 743 cm^{-1} to the δsCF_3 mode and the weaker line at 830 cm^{-1} to νaSNS.

Theoretical Results and Discussion

Structure. In our earlier calculations,[13] two stable rotamers of C_1 and C_2 symmetry were obtained for the TFSI anion. The calculated structures of the more stable C_2 rotamer of $TFSI^-$ and of free HTFSI are given in Figure 6. The geometry

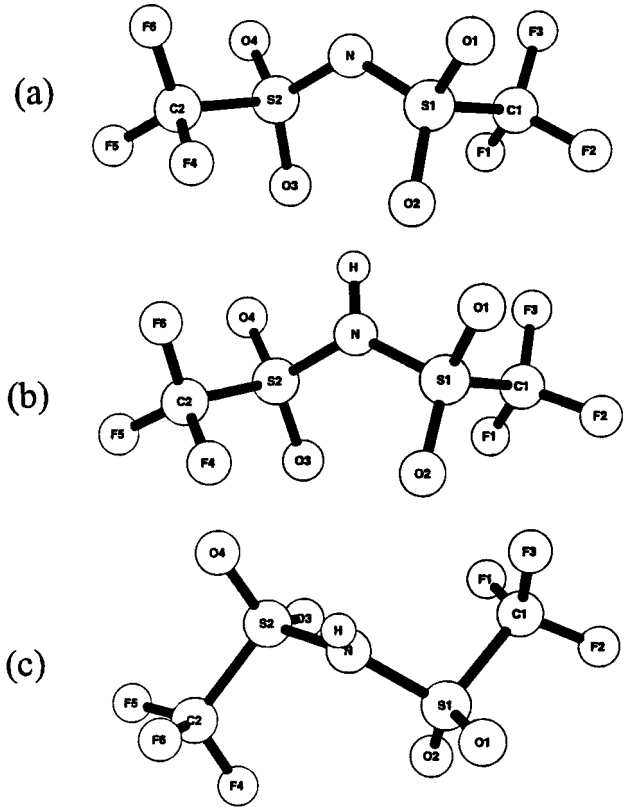

Figure 6. Calculated structures of the free $TFSI^-$ anion (a) and HTFSI molecule (b). In (c), the HTFSI molecule is shown from another angle.

TABLE 4: Selected Bond Geometry Parameters for the TFSI Anion and the HTFSI Acid[a]

	$TFSI^-$		HTFSI	
	calcd ref 13	exptl ref 33	calcd this work	exptl ref 33
r(C−F1)	1.313	1.296	1.300	1.298
r(C−F2)	1.318	1.308	1.303	1.307
r(C−F3)	1.314	1.249	1.307	1.330
r(C−S)	1.820	1.812	1.825	1.840
r(S−O1)	1.430	1.418	1.411	1.401
r(S−O2)	1.431	1.407	1.416	1.417
r(S−N)	1.575	1.576	1.660	1.644
r(N−H)			1.003	0.990
a(S−C−F1)	111.5	110.9	110.5	
a(S−C−F2)	109.5	110.7	107.9	
a(S−C−F3)	111.2	110.6	108.9	
a(O−S−O)	118.5	119.4	124.0	123.9
a(O1−S−N)	109.2	107.8	109.6	109.1
a(O2−S−N)	116.0	116.0	104.9	106.9
a(C−S−N)	102.9	104.0	102.2	102.2
a(S−N−S)	127.8	125.0	130.5	128.4
a(H−N−S)			114.8	115.8
d(O1−S−N−S)	−157.9		−160.7	
d(O2−S−N−S)	−20.7		−25.6	
d(C−S−N−S)	92.7		88.6	
d(C−S−N−H)			−91.4	

[a] Bond lengths (*r*) in Å and bond angles (*a*, *d*) in deg.

parameters (Table 4) compare as a whole very favorably with the experimentally determined ones (Table 3). In particular, the agreement between the calculated and experimentally determined SNS angles is important since this bond angle as obtained by Arnaud et al.[12] was about 30° larger than the present value. They used a smaller basis set with diffuse functions, and in order to test the basis set dependence diffuse functions were also used with the 6-31G* basis set in ref 13 on the TFSI anion. No large differences as compared to the result using 6-31G* were found, and we therefore conclude that the basis sets used in the present calculations give a faithful description of the molecules.

TABLE 5: Mulliken Charges for the TFSI Anion and the HTFSI Acid

atom	TFSI (13)	HTFSI	atom	TFSI (13)	HTFSI
H		0.40	C	0.83	0.86
N	−0.94	−1.01	F1	−0.34	−0.30
S	1.52	1.59	F2	−0.35	−0.31
O1	−0.68	−0.60	F3	−0.34	−0.32
O2	−0.67	−0.61			

Two of the experimental C−F bond distances in $TFSI^-$ are, however, about 0.05 Å shorter than the other ones and differ from the calculated ones with the same amount. If we consider the thermal parameters given in ref 33, Table 4, it is found that for the two fluorines involved in these bonds the mean-square amplitude values, U_{eq}, are twice as large as for the other fluorines in the crystal structure. This indicates some kind of disorder, which would lead to an apparent shortening of the C−F bond distances.

Charge Distributions. Our calculations on free $TFSI^-$ or HTFSI give also some insight into the charge distributions. They are given by the Mulliken charges reported in Table 5. It is seen that the negative charge on the nitrogen is larger than the charges on the oxygens, in agreement with the fact that the proton resides on the nitrogen in HTFSI. In solid LiTFSI[7] the cation is, however, coordinated to the oxygen atoms despite the larger negative charge on nitrogen. The possibility for the larger divalent cations Ca^{2+}, Sr^{2+}, and Ba^{2+} to coordinate to one of the oxygens and the nitrogen atom has been suggested.[9]

Vibrational Frequencies and Intensities. The calculated data are reported in Table 6 for $TFSI^-$ and in Table 7 for HTFSI. Finally, the internal force constants are given in Table 8. The potential energy distribution (PED) contributions given in Tables 6 and 7 and used in the text show the contribution of each internal coordinate to the potential energy of the normal modes. The notation A−B is used for stretching coordinates involving atoms A and B, A−B−C for bending coordinates involving atoms A, B, and C, and, finally, A−B−C−D used for torsional coordinates about the B−C bond involving atoms A, B, C, and D. The PED contributions given are sums over all internal coordinates with the same notation in order to condense the tables, and therefore, no numbering of the atoms is used.

Comparison of Calculated and Experimental Spectra

The TFSI Anion. The calculated and experimental IR and Raman spectra are compared in Figure 7. Let us recall that two different rotamers of C_1 and C_2 symmetry were previously found,[13] the C_2 one being more stable by only 2.3 kJ/mol. These rotamers differ in their vibrational pattern mainly in the region below 700 cm^{-1}. We have restricted our presentation to the C_2 rotamer in order to facilitate the comparison with HTFSI.

It is seen in Figure 7 that the calculations are moderately successful in predicting the frequencies and intensities of the experimental IR bands we have previously assigned to the ν_a-SO_2 and $\nu_a CF_3$ vibrations. Similar problems were encountered for the SO_3 and especially for the CF_3 stretching frequencies calculated for the $CF_3SO_3^-$ anion,[43] and these problems remained also when electron correlation effects were taken into account. Let us note, however, that although the absolute positions of the experimental and calculated bands differ considerably a $\nu_a SO_2$ mode splitting of 25 cm^{-1} is calculated, with $\nu_a^{i.p.}SO_2$ (A) higher than $\nu_a^{o.p.}SO_2$ (B), in very good

TABLE 6: Vibrational Frequencies, IR Intensities, and Raman Activities for the C2 Rotamer of the TFSI Anion

ν (cm^{-1}) unscaled	ν ($\times 0.90$) scaled	IR int. (km mol^{-1})	Raman act. ($Å^4$ amu^{-1})	mode (% of PED)	sym.
35	31	2.4	0.0	C−S−N−S (90)	A
52	45	0.2	0.0	C−S−N−S (55); F−C−S−N (39)	A
54	48	2.5	0.0	F−C−S−N (50); C−S−N−S (43)	B
60	53	0.1	0.0	F−C−S−N (96)	B
127	113	0.0	0.6	C−S−N (58); C−S−O (8)	A
175	158	0.3	0.1	S−N−S (74); N−S−O (11)	A
220	198	4.9	0.0	C−S−O (52); F−C−S (44)	A
228	205	0.9	0.1	C−S−O (49); F−C−S (46)	B
252	227	16.5	0.0	F−C−S (47); C−S−N (21); C−S−O (16)	B
306	276	0.1	4.0	F−C−S (50); C−S (19)	A
320	288	1.2	2.4	N−S−O (60); C−S−O (16)	B
345	311	0.7	3.9	C−S−O (24); N−S−O (22); C−S (20); S−N (13)	A
361	325	0.5	0.0	C−S (48); F−C−S (19); F−C−F (10)	B
376	339	0.2	2.6	F−C−S (34); C−S−O (18); O−S−O (13); C−S (10)	A
399	360	3.8	0.6	C−S−N (38); F−C−S (20); N−S−O (7)	B
432	389	8.9	3.0	F−C−S (19); S−N (18); N−S−O (15); C−S−O (15)	A
448	403	10.2	2.1	N−S−O (29);C−S−O (23);F−C−S (23);F−C−F (20)	B
564	507	93.6	0.1	O−S−O (30); F−C−F (27); N−S−O (16)	B
584	526	0.1	0.6	F−C−F (45);F−C−S−N (21);O−S−O (9)	A
603	541	4.0	1.8	F−C−F (43);F−C−S−N (30)	A
612	549	0.3	1.9	F−C−F (39);F−C−S−N (25); C−F (14)	B
631	568	79.6	2.6	O−S−O(22);F−C−S−N(18);N−S−O (10);C−S−N (9)	B
654	590	0.0	1.7	O−S−O(37); C−S−N (14); C−S−O (8)	A
703	633	431.0	0.0	C−S−O(30); C−S−N(16); N−S−O(16)	B
703	634	66.2	2.4	N−S−O(48); C−S−O(14); S−N−S(11)	A
815	733	32.5	16.7	S−N(32); N−S−O(12); F−C−S(8); C−F(7)	A
854	767	32.6	0.0	C−F(53); C−S(16)	B
875	786	20.6	1.2	C−F(38); S−N(20); C−S(13); N−S−O(10)	A
1179	1062	491.9	0.0	S−O(49); S−N(36)	B
1256	1131	11.7	11.7	S−O(77); S−N(6)	A
1271	1145	573.3	0.6	S−N(47); S−O(41)	B
1377	1241	149.6	1.6	C−F (79)	A
1379	1243	472.8	0.5	C−F (77)	B
1386	1249	128.8	0.9	C−F (77)	A
1392	1255	286.9	1.2	C−F (75)	B
1416	1274	314.5	0.1	C−F(41); C−S(19); S−N(11)	B
1417	1275	2.4	10.3	C−F(39); C−S(22); F−C−F(15)	A
1443	1300	158.6	3.3	S−O (95)	B
1472	1325	732.0	1.2	S−O (89)	A

agreement with our qualitative assignment and observed splitting of 20−24 cm^{-1} (Table 1). The calculated values for the $\nu_s SO_2$ and $\nu_a SNS$ modes are in better agreement with the experimental values, but the %PED values of Table 6 reveal a rather strong coupling between $\nu_a SNS$ and $\nu_a^{o.p.} SO_2$ of B symmetry. On the other hand, the $\nu_s^{i.p.} SO_2$ mode of A symmetry is mainly involved in the intense and polarized Raman line observed at 1132−1137 cm^{-1} and calculated at 1131 cm^{-1}.

Another intriguing problem is the PED description for the more intense Raman line observed at about 740 cm^{-1}. According to many literature examples of derivatives involving the CF_3 or SCF_3 groups, such an intense Raman line has always been assigned to the $\delta_s CF_3$ mode, even if coupling with the C−S stretching has often been invoked.[29,30,44] The corresponding vibration, calculated at 733 cm^{-1}, is described in the PED as a complex mixing of internal coordinates, but with no F−C−F bending contribution among the four largest ones (Table 6). With the aid of a visualization of this motion, it is seen that the whole molecule is expanding and contracting, in agreement with the PED prediction of many medium large contributions besides the SN stretching coordinates. From this description one could easily envisage a large polarizability change accompanying the vibration and accordingly an intense Raman band. A similar situation was encountered by Huang et al.[45] for the triflate ion. These authors observe an intense Raman line at 754 cm^{-1} and assign it to $\delta_s CF_3$ with a significant contribution of νCS. However, their calculated PEDs reveal a predominant C−F stretching contribution (53%), accompanied by many other contributions (C−S 13%, F−C−F 13%, F−C−S 11%, O−C−S 6%). They have no further comment on this problem.

In our calculation, large contributions to the PEDs (=39%) from the F−C−F bending coordinates occur for the modes at 549, 541, and 526 cm^{-1}. Visualization of these modes reveal that a classification in terms of $\delta_s CF_3$ and $\delta_a CF_3$ (with imagined approximate C_3 axes through the C and S atoms) is not possible. Rather a decoupling of the three C−F bonds occurs where either one or two of the C−F bonds take part in bending motions. This behavior would in fact imply approximate mirror planes through the atoms F_2, C_1, and S_1 at one end and F_5, C_2, and S_2 at the other end (Figure 6).

Another problem comes from the experimental IR frequencies at 763 and 790 cm^{-1}, qualitatively assigned in Table 1 as ν_s-SNS and νCS, respectively. They also appear in Table 6 as strongly mixed C−F, S−N, and C−S stretching coordinates. Thus, the PEDs of the modes occurring between 730 and 790 cm^{-1} indicate that a qualitative description in terms of group vibrations is very approximate.

Below 700 cm^{-1}, the agreement between calculated and experimental values is much better, and in this case, the calculated PED is very helpful to describe the different modes as strong couplings are systematically involved.

The HTFSI Molecule. The comparison given in Figure 5 is much more satisfactory than for the anion. Most of the previous problems have disappeared, except for the $\nu_a SO_2$ modes, which are again calculated at lower frequencies than

TABLE 7: Vibrational Frequencies, IR Intensities, and Raman Activities for the HTFSI Acid

ν (cm^{-1}) unscaled	ν ($\times$0.90) scaled	IR int. (km mol^{-1})	Raman act. ($Å^4$ amu^{-1})	mode (% of PED)	sym.
33	30	0.4	0.0	F−C−S−N (37); C−S−N−S (34); H−N−S−C (22)	A
45	41	0.2	0.0	C−S−N−S (55); F−C−S−N (33); H−N−S−C (10)	B
52	47	0.1	0.0	F−C−S−N (70); C−S−N−S (13); H−N−S−C (12)	A
64	58	0.7	0.0	F−C−S−N (56); C−S−N−S (42)	B
119	107	0.0	0.5	C−S−N (59)	A
167	150	3.4	0.1	S−N−S (45); H−N−S (22); N−S−O (22)	A
217	195	3.8	0.5	C−S−O (49); F−C−S (36)	B
220	198	7.0	0.1	C−S−O (53); F−C−S (43)	A
226	203	19.1	0.2	F−C−S (47); C−S−N (28); C−S−O (12)	B
280	252	5.0	1.3	N−S−O (61); F−C−S (9); H−N−S−C (8)	B
293	264	0.1	4.2	F−C−S (44); S−N (15); C−S (13); N−S−O (10)	A
327	294	2.3	4.0	N−S−O (32); C−S (19); S−N (18); C−S−O (16)	A
359	323	0.9	0.0	C−S (53); N−S−O (9)	B
371	334	0.2	5.1	F−C−S (26); C−S (19); O−S−O (18); F−C−F (10)	A
389	350	3.6	0.2	C−S−N (38); F−C−S (25); O−S−O (8)	B
412	371	9.2	1.6	F−C−S (34); C−S−O (30); F−C−F (14); S−N (10)	A
421	379	1.3	2.1	C−S−O (35); F−C−S (31);F−C−F (15)	B
516	464	56.8	1.4	H−N−C−S (78); N−S−O (9)	B
553	498	123.2	0.3	O−S−O (33); N−S−O (26); F−C−F (16)	B
578	520	1.1	0.7	F−C−F (44);F−C−S−N (19); O−S−O (13); N−S−O (9)	B
605	545	2.3	1.2	F−C−F (40); F−C−S−N (29); C−F (9)	A
610	549	0.5	2.1	F−C−F (41); F−C−S−N (25); C−F (11)	B
628	565	43.7	1.9	F−C−S−N (21); F−C−F (19); O−S−O(15); C−S−N (10)	B
645	581	0.0	2.1	O−S−O (36); C−S−N(12); C−S−O (6)	A
692	623	501.3	0.0	C−S−O (31); N−S−O(20); O−S−O(10); C−S−N (8)	B
695	626	5.8	0.3	N−S−O(42); C−S−O (17); F−C−S(8); S−N−S (6)	A
850	765	8.9	17.0	C−F(36); C−S(11); S−N (10)	A
865	779	2.5	0.0	C−F(50); C−S (17)	B
908	817	28.8	0.8	S−N (34); N−S−O (22)	A
980	882	518.2	1.0	S−N (85); H−N−S (7)	B
1251	1126	522.5	1.4	S−O (65); C−F (13)	B
1258	1132	0.9	10.9	S−O (54); C−F (19)	A
1382	1244	217.2	0.6	C−F (37); S−O (22); C−S (16)	B
1400	1260	5.1	12.3	C−F (67)	A
1432	1289	332.3	1.8	C−F (75)	A
1433	1290	99.8	0.6	C−F(51); S−O (22)	B
1447	1302	10.8	0.7	C−F (68)	A
1451	1306	468.8	0.5	C−F (84)	B
1483	1335	49.1	2.7	H−N−S (57); S−O (37)	B
1566	1409	584.9	1.2	S−O (95)	A
1580	1422	207.5	1.2	S−O (63); H−N−S (32)	B
3789	3410	167.6	36.1	N−H (100)	A

the experimental ones. Furthermore, the modes at 1422 and 1335 cm^{-1} (of B symmetry) are found to consist of coupled ν_aSO_2 and δNH coordinates. This coupling is somewhat different from those mentioned above, since there are no bonds in common in the definition of the NH in-plane bending and the S−O stretching coordinates. The SO_2 mode of A symmetry at 1409 cm^{-1} is on the other hand almost pure. In the IR spectrum of gaseous HTFSI, a strong band at 1463 cm^{-1} accompanied by a shoulder at 1440 cm^{-1} might contain both A and B type SO_2 stretching mode contributions. Let us recall that the corresponding mode in $TFSI^-$ is calculated to 1300 cm^{-1}. This increase in stretching frequency for HTFSI is reflected in the S−O force constants, which show an average increase of 20% for HTFSI relative to TFSI (Table 8).

The CF stretching frequencies are better reproduced and, in particular, the well-isolated and intense Raman line observed at 1250 cm^{-1} is calculated at 1260 cm^{-1} as a nearly pure ν_sCF_3 (A). The same kind of observation can be made for the ν_sSO_2 and ν_aSNS vibrations.

The most intense Raman line observed and calculated at 765 cm^{-1} and assigned as δ_sCF_3 on the basis of comparisons with other molecules corresponds again to a normal mode with the dominating contribution to the PED from the C−F, C−S, and S−N stretching coordinates and not from F−C−F bending ones (cf. Table 7). The latter appear with important PED contributions for the modes at 549, 545, and 520 cm^{-1} as in the case of the anion, and we have nothing to add to the previous comments.

As already pointed out, the comparison between calculated and experimental values is quite valid for the gas phase but more questionable for the solid phase. An obvious effect of intermolecular forces is the shift of the νNH frequency from about 3400 cm^{-1} (calculated and measured for gaseous HTFSI) to 3200 cm^{-1} in the solid (Table 1). It seems, however, that the other internal modes of HTFSI are not strongly perturbed in the solid state.

Conclusion

One of the main objectives of this work was to reconcile previous discrepancies in the vibrational assignments[10,14] and calculated geometry[12,13] of the $TFSI^-$ anion. The comparison between the IR and Raman spectra of the solvated anion and of the HTFSI molecule has confirmed our previous assignments for the important stretching modes of the SO_2, CF_3 and SNS groups.[14] The calculations have confirmed that the SNS angle in these systems is about 128−130°, in agreement with the values found by diffraction techniques.

Problems remain, however, in the comparison between the calculated and experimental frequencies and intensities, particularly for the anion and for the ν_aSO_2, νCF_3, and δ_sCF_3

TABLE 8: Internal Force Constants for the TFSI Anion and the HTFSI Acid

force constant ($N \cdot m^{-1}$)	TFSI	HTFSI
Stretchings		
N−H		781
S−N	677	516
S−O1	1144	1297
S−O2	1157	1275
C−S	414	396
C−F1	809	827
C−F2	785	818
C−F3	805	802
Bendings[a]		
H−N−S		28
S−N−S	49	24
O1−S−N	63	61
O2−S−N	65	62
O−S−O	65	59
C−S−N	51	46
O1−S−C	52	47
O2−S−C	57	50
F1−C−S	38	40
F2−C−S	37	38
F3−C−S	38	40
F1−C−F2	49	50
F2−C−F3	50	49
F1−C−F3	50	50
Torsions[b]		
H−N−S−C		5
F1−C−S−N	14	13
F2−C−S−N	14	13
F3−C−S−N	15	13
C−S−N−S	7	4

[a] Normalized with the factor $(r_1r_2)^{-1}$. [b] Normalized with the factor $(r_1r_3)^{-1}$.

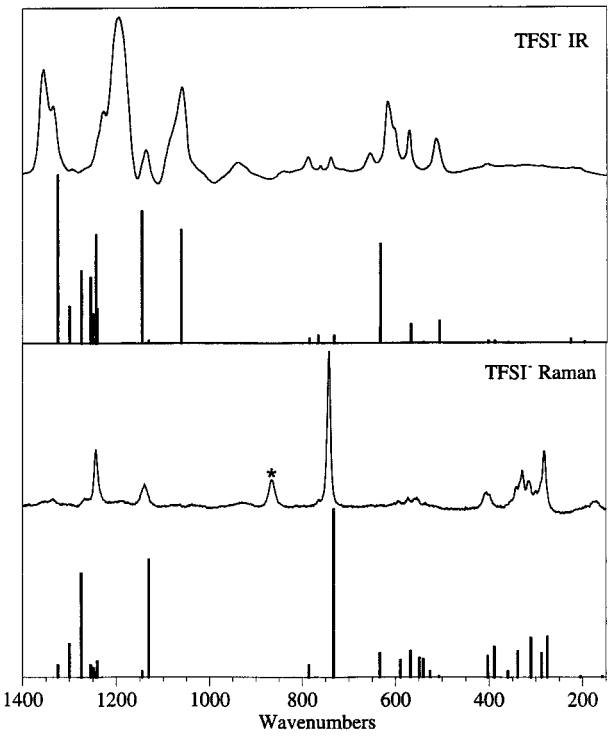

Figure 7. Comparison of the experimental and calculated IR and Raman spectra of the $TFSI^-$ anion. The experimental IR spectrum is taken from Figure 3c and the Raman one from Figure 3f. The asterisk in the latter indicates a line not due to the anion but coming from the PEO breathing mode.

modes. We have considered for simplicity the more stable C_2 rotamer of $TFSI^-$, but the C_1 rotamer is rather close in energy and one can infer that fast conformational dynamics occur in the free anion. This could lead to a very anharmonic potential along the coordinate involved in the C_2/C_1 exchange (rotation about the SN bonds), the SNS group being rather rigid. The calculation of such a fluxional system could be the next step to achieve a better agreement with the experimental data.

References and Notes

(1) Armand, M.; Gorecki, W.; Andréani, R. In *Second International Symposium on Polymer Electrolytes*; Scrosati, B., Ed.; Elsevier Applied Science: New York; 1990, p 91.

(2) Gorecki, W.; Jeannin, M.; Belorizki, E.; Roux, C.; Armand, M. *J. Phys. Condens. Matter* **1995**, *7*, 6823.

(3) Vallée, A.; Besner S.; Prud'homme, J. *Electrochim. Acta* **1992**, *37*, 1579.

(4) Paul, J.-L.; Jegat, C.; Lassègues, J.-C. *Electrochim. Acta* **1992**, *37*, 1623.

(5) Hernandez, M.; Servant, L.; Grondin, J.; Lassègues, J.-C. *Ionics* **1995**, *1*, 454.

(6) Lascaud, S.; Perrier, M.; Vallée, A.; Besner, S.; Prud'homme, J.; Armand, M. *Macromolecules* **1994**, *27*, 7469.

(7) Nowinski, J. L.; Lightfoot, P.; Bruce, P. G. *Mater. Chem.* **1994**, *4*, 1579.

(8) Andreev, Y. G.; Lightfoot, P.; Bruce, P. G. *Chem. Commun.* **1994**, 2169.

(9) Bakker, A.; Gejji, S.; Lindgren, J.; Hermansson, K.; Probst, M. M. *Polymer* **1995**, *36*, 4371.

(10) Wen, S. J.; Richardson, T. J.; Ghantous, D. J.; Strickel, K. A.; Ross P. N.; Cairns, E. J. *J. Electroanal. Chem.* **1996**, *408*, 113.

(11) Abbrent, S.; Lindgren, J.; Tegenfeldt, J.; Wendsjö, Å. *Electrochim. Acta*, in press.

(12) Arnaud, R.; Benrabah, D.; Sanchez, J.-Y. *J. Phys. Chem.* **1996**, *100*, 10882.

(13) Johansson, P.; Gejji, S. P.; Tegenfeldt, J.; Lindgren, J. *Electrochim. Acta*, in press.

(14) Rey, I.; Lassègues, J.-C.; Grondin, J.; Servant, L. *Electrochim. Acta*, in press.

(15) Foropoulos, J.; DesMarteau, D. D. *Inorg. Chem.* **1984**, *23*, 3720.

(16) Frisch, M. J.; Trucks, G. W.; Schlegel, H. B.; Gill, P. M. W.; Johnson, B. G.; Robb, M. A.; Cheeseman, J. R.; Keith, T.; Petersson, G. A.; Montgomery, J. A.; Raghavachari, K.; Al− Laham, M. A.; Zakrzewski, V. G.; Ortiz, J. B.; Foresman, J. B.; Cioslowski, J.; Stefanov, B. B.; Nanayakkara, A.; Challacombe, M.; Peng, C. Y.; Ayala, P. Y.; Chen, W.; Wong, M. W.; Andres, J. L.; Replogle, E. S.; Gomperts, R.; Martin, R. L.; Fox, D. J.; Binkley, J. S.; Defrees, D. J.; Baker, J.; Stewart, J. P.; Head-Gordon, M.; Gonzalez, C.; Pople, J. A. *GAUSSIAN 94, Revision B.2*, Gaussian Inc.: Pittsburgh, PA, 1995.

(17) Schmidt, M. W.; Baldridge, K. K.; Boatz, J. A.; Elbert, S. T.; Gordon, M. S.; Jensen, J. H.; Koseki, S.; Matsunaga, N.; Nguyen, K. A.; S. Su, Windus, T. L.; Dupuis M.; Montogomery, J. A., Jr. *J. Comput. Chem.* **1993**, *14*, 1347.

(18) *Spartan, version 4.1*, Wavefunction Inc., 1995.

(19) *Polymer Electrolytes Reviews*; MacCallum, J. R., Vincent, C. A., Eds.; Elsevier Applied Science: London and New York, 1989; Vol. 2, p 43.

(20) Gray, M. F. *Solid Polymer Electrolytes: Fundamentals and Technological Applications*; VCH Publishers: New York, 1991.

(21) Gray, M. F. *Polymer Electrolytes*; RSC Materials Monographs; Connor J. A., Series Ed.; The Royal Society of Chemistry: Cambridge, 1997.

(22) Ferry, A.; Jacobsson, P.; Torell, L. M. *Electrochim. Acta* **1995**, *40*, 2369.

(23) Rey, I. Thesis, University Bordeaux I, France, 1997.

(24) Lasssègues, J.-C.; Bruneel, J.-L.; Grondin, J.; Rey, I.; Servant, L.; Vigneau, L. *Mol. Cryst. Liq. Cryst.*, in press.

(25) Rey, I.; Bruneel, J.-L.; Grondin, J.; Servant, L.; Lassègues, J.-C. *J. Electrochem. Soc.*, in press.

(26) Sawyer, J. F.; Schrobilgen, G. J.; Sutherland, S. J. *Inorg. Chem.* **1982**, *21*, 4064.

(27) Von Blaschette, A.; Bürger, H. *Z. Anorg. Allg. Chem.* **1970**, *378*, 104.

(28) Katsuhara, Y.; Hammaker, R. M.; Desmarteau, D. D. *Inorg. Chem.* **1980**, *19*, 607.

(29) Dollish, F. R.; Fateley, W. G.; Bentley, F. F. *Characteristic Raman Frequencies of Organic Compounds*; John Wiley and Sons: New York, 1974.

(30) Linvien, D.; Colthup, N. B.; Fateley, W. G.; Grasselli, J. G. *The Handbook of Infrared and Raman Characteristic Frequencies of Organic Molecules*; Academic Press: London, 1991.

(31) Papke, B. L.; Ratner, M. A.; Shriver, D. F. *J. Phys. Chem. Solids* **1981**, *42*, 493.
(32) Papke, B. L.; Ratner, M. A.; Shriver, D. F. *J. Electrochem. Soc.* **1982**, *129*, 1434.
(33) Haas, A.; Klare, Ch.; Betz, P.; Bruckmann, J.; Kruger, C.; Tsay, Y.-H.; Aubke, F. *Inorg. Chem.* **1996**, *35*, 1918.
(34) Koppel, I. A.; Taft, R. W.; Anvia, F.; Zhu, S. Z.; Hu, L. Q.; Sung, K. S.; Desmarteau, D. D.; Yagupolskii, L. M.; Yagupolskii, Y. L.; Ignatev, N. V.; Kondratenko, N. V.; Volkonskii, A. Y.; Vlasov, V. M.; Notario, R.; Maria, P. C. *J. Am. Chem. Soc.* **1994**, *116*, 3047.
(35) Von Blaschette, A.; Schomburg, D.; Wieland, E. Z. *Z. Anorg. Allg. Chem.* **1989**, *571*, 75.
(36) Attig, R.; Mootz, D. *Acta Crystallogr.* **1975**, *B31*, 1212.
(37) Von Blaschette, A.; Wieland, E.; Schomburg, D.; Adelhelm, M. *Anorg. Allg. Chem.* **1986**, *533*, 7.
(38) DesMarteau, D. D.; Zuberi, S. S.; Pennington, W. T.; Randolph, B. B. *Eur. J. Solid State Inorg. Chem.* **1992**, *29*, 777.
(39) Cotton, F. A.; Stokely, P. F. *J. Am. Chem. Soc.* **1970**, *92*, 294.
(40) Sawyer, J. F.; Schrobilgen, G. J.; Sutherland, S. J. *Inorg. Chem.* **1982**, *21*, 4064.
(41) Isenberg, W.; Noltemayer, M.; Sheldrick, G. M. *Acta Crystallogr.* **1982**, *B38*, 2887.
(42) Müller-Plathe, F.; van Gunsteren, W. F. *J. Chem. Phys.* **1995**, *103*, 4745.
(43) Gejji, S. P.; Hermansson, K.; Lindgren, J. *J. Phys. Chem.* **1993**, *97*, 6986.
(44) Huang, W.; Frech, R.; Wheeler, R. A. *J. Phys. Chem.* **1994**, *98*, 100.
(45) Huang, W.; Wheeler, R. A.; Frech, R. *Spectrochim. Acta* **1994**, *50A*, 985.